Electrochimica Acta 74 (2012) 207–214

Contents lists available at SciVerse ScienceDirect

Electrochimica Acta

journal homepage: www.elsevier.com/locate/electacta

Excellent electrochemical performance of graphene-silver nanoparticle hybrids prepared using a microwave spark assistance process

A.M. Shanmugharaj, Sung Hun Ryu *

Department of Chemical Engineering, Kyung Hee University, Yongin, Kyunggi-Do 446701, South Korea

ARTICLE INFO

Article history:
Received 27 January 2012
Received in revised form 15 April 2012
Accepted 16 April 2012
Available online 23 April 2012

Keywords:
Graphene
Silver nanoparticles
Microwave radiation
Anode materials
Specific capacity

ABSTRACT

A simple method is described for the synthesis of graphene-silver nanoparticle hybrids from graphite and silver precursors using microwave spark ignition process. Adding ecofriendly free radical initiators, in the presence of hydrogen peroxide solution leads to the expansion of graphite to graphene nanosheets. Simultaneously, silver ions intercalated between the graphene layers are reduced to silver nanocrystals leading to the development of graphene-silver nanoparticle hybrids. Transmission electron microscopic (TEM) studies reveal the successful formation of graphene-silver nanoparticle hybrids. X-ray diffraction (XRD) shows that the silver nanoparticles formed on the graphene surfaces are face centered cubic crystals. The surface composition and functional groups present on the graphene-silver nanoparticle hybrids are corroborated using X-ray photoelectron spectroscopy (XPS) and Fourier Transform Infrared Spectroscopy (FT-IR). The lithium storage capacity of the synthesized material, when used as an anode material for rechargeable lithium secondary batteries is investigated. Its first specific discharge capacity is observed to be 580 mAh g^{-1} and this has been increased to 827 mAh g^{-1}, by incorporating the silver nanoparticles between the graphene platelets. The reversible capacity of the graphene-silver nanoparticle hybrids is observed to be 714 mAh g^{-1}, which is significantly higher compared to that of graphene (420 mAh g^{-1}) prepared by the same process.

1. Introduction

Graphene is a two dimensionally arranged single layer carbon atoms in a hexagonal lattice and it is one of the few structures that are stable in two dimensions [1]. Graphene sheets have attracted considerable interest in recent years as the atomic-scale scaffold for design of new nanomaterials because of its extraordinary properties, such as high carrier mobility, half-integer quantum hall effect at room temperature [2], spin transport [3], high elasticity [4], electromechanical modulation and ferromagnetism [5]. Many kinds of graphene-based devices have been fabricated such as field effect transistor [6], non-volatile memory [7], transparent electrode [8], gas sensor [9], and electrode materials for energy storage devices [10–12].

Graphite is commonly used as an anode material in energy storage devices such as lithium-ion batteries due to its high columbic efficiency (the ratio of the extracted lithium to the inserted lithium) and relatively low cost. But six carbon atoms are required to accommodate each lithium ion, resulting in a relatively low specific capacity (372 mAh g^{-1}). To achieve higher lithium storage capacities, many metals and metal oxides such as silicon (Si, 4200 mAh g^{-1}), germanium (Ge, 1600 mAh g^{-1}), tin (Sn, 990 mAh g^{-1}), silver (Ag, 820 mAh g^{-1}), tin(II) oxide (SnO_2, 790 mAh g^{-1}), nickel oxide (NiO, 718 mAh g^{-1}) and cobalt oxide (Co_3O_4, 890 mAh g^{-1}) have been developed as advanced anode materials to replace graphite [13–19]. A major challenge, when employing these substances as anode materials is that they suffer from large volume variation (up to 400%) during the lithium insertion/extraction process, which leads to the pulverization of the electrode and thereby rapid decay in the specific capacity [20].

One possible approach to solve this problem is to make graphene-nanoparticle hybrids. In the anodes of lithium ion batteries (LIBs), graphene sheets can acts as matrices for metal and metal oxide nanoparticles that greatly enhance the cyclic performance of the electrodes. Significant research has been done in the development of three dimensional (3D) arrays of graphene-nanoparticle hybrids. For instance, hybrids consisting of 3D array of graphene-silicon nanoparticle exhibit high lithium storage capacity and cycling stability (>1500 mAh g^{-1} after 200 cycles) compared graphite or silicon based anode materials [21]. Although, graphene buffers the changes in nanoparticle volume well, nanoparticles are still prone to aggregation upon cycling. To overcome this issue, confinement of individual nanoparticles on graphene shell is necessary, which can be achieved through in situ synthetic approaches using nanoparticle precursors. Wang et al. [22] applied this method to get homogenous distribution of Sn nanoparticles in graphene sheets.

* Corresponding author. Tel.: +82 312012534; fax: +82 312021946.
E-mail address: shryu@khu.ac.kr (S.H. Ryu).

0013-4686/$ – see front matter © 2012 Elsevier Ltd. All rights reserved.
http://dx.doi.org/10.1016/j.electacta.2012.04.057

These anode materials showed enhanced capacity and reversibility (508 mAh g^{-1} for 100 cycles) compared to electrodes prepared using bare graphene (255 mAh g^{-1} for 100 cycles) or Sn nanoparticles (failed in 10 cycles). Recently, Yang et al. [23] synthesized graphene encapsulated Co_3O_4 anode materials with remarkable lithium storage performance, self assembled through electrostatic forces.

Generally, graphene nanosheets used for synthesis of these graphene-nanoparticle hybrids are prepared through physical, electrochemical or chemical methods in which individual graphene layers were extracted from graphite, carbon fibers or carbon nanotubes [24]. Most of the chemical methods reported till dates rely heavily on the usage of harsh oxidizers like H_2SO_4/$KMnO_4$ [24] or formic acid [25]. Recently, synthesis of graphene has been done through eco-friendly route using microwave radiation [26]. Though graphene synthesis through eco-friendly route has received lot of attention because of their unique properties, no report is available on the direct synthesis of graphene-nanoparticle hybrids using microwave radiation. In the present study, we report a novel one pot synthesis route to prepare graphene-metal nanoparticle hybrids using ecofriendly microwave radiation and characterized the electrochemical performances of the resultant nanoparticle hybrids.

2. Experimental

2.1. Materials

Natural graphite, hydrogen peroxide (H_2O_2), ammonium peroxidisulfate ($(NH_4)_2S_2O_8$), silver nitrate ($AgNO_3$, 99% purity) and poly(ethylene glycol) (PEG) were procured from Sigma–Aldrich, Korea and used without further purification. Distilled water used in this study was prepared by an ultrapure water purification system (Sartorius AG, Germany).

2.2. Microwave spark ignition assisted graphene synthesis

Natural graphite (2 g) was mixed with 30% (w/w in water) H_2O_2 (4 g) and ammonium peroxidisulfate (0.1 g) in the ratio of 1:2:0.1 (w/w). To this the desired quantity of silver nitrate solution (0.0025 M) was added followed by the addition 25 mL of poly (ethylene glycol) solution (1 wt% in distilled water). The resultant mixture was transferred to a vial and subjected to microwave irradiation (domestic microwave oven, 700 W) for 60 s, resulting in bright sparks and an intense heat release resulting in the evaporation of water. The vial was subjected to cooling at every 20 s irradiation time to prevent the breaking of vial. The graphene-silver nanoparticle hybrids were obtained from the treated graphite after repeated washing with water, sonication and centrifugation.

2.3. Characterization

The synthesized graphene and its nanoparticle hybrid samples were deposited onto a carbon coated copper grid, dried and observed by transmission electron microscope (TEM, JEM-2100F, JEOL), powder samples were analyzed using X-ray diffractometer (XRD, D8 Advance, Bruker). Raman spectroscopic studies were performed using Raman spectrometer (RFS-100/S, Bruker), recorded at room temperature by using 514 nm laser excitation. Surface elemental compositions of graphene and graphene-silver nanoparticle hybrids were determined using X-ray photoelectron spectroscopy (XPS, K-Alpha, Thermoelectron). The samples for XPS measurements were prepared by casting the graphene dispersants (dispersed in ethanol) onto silicon wafer followed by drying under vacuum at 70 °C. The synthesized graphene nanoparticle hybrids were also characterized by Fourier Transform Infrared Spectroscopy (FT-IR, Spectrum one, Perkin-Elmer) in KBr matrix. Thermogravimetric analysis (TGA) of graphene-silver nanoparticle hybrid was characterized in the temperature range of 25–800 °C at the heating rate of 10 °C/min in air environment using TA instruments (TGA Q5000 IR/SDT Q600).

2.4. Electrode preparation and coin type cell fabrication

The electrochemical performances of Li-ion anode materials based on graphene nanoparticle hybrids were measured by fabricating 2032-type Li-ion half cells. Electrodes were prepared by casting a slurry with a composition of 90 wt% graphene nanoparticle hybrid, 5 wt% of super P (TIMCAL) and 5 wt% of PVDF binder (Kureha KF100) onto a copper current collector foil. The slurry was prepared by grinding the mixture in the presence of N-methyl pyrrolidone solvent using mortar for 15 min. The viscous slurry coated onto copper foil was dried in oven at 100 °C for 5 h followed by punching out 14 mm diameter samples. The electrode was assembled into coin type cell with 1 M $LiPF_6$ solution in a 1:1 (volume) mixture of ethylene carbonate (EC) and dimethyl carbonate (DMC) (Merck Co.,) as electrolyte. Metallic lithium was used as the counter and reference electrodes in the electrochemical cell assembly.

2.5. Electrochemical measurements

Electrochemical properties of the coin type cells were measured by galvanostatically charging/discharging the batteries in the voltage range of 0.01–3.0 V vs. Li/Li^+ using Wonatech battery analyzer. Cyclic voltammetry curves were measured at 0.1 mV s^{-1} within the range of 0.01–3 V using an electrochemical work station (CHI 660C).

3. Results and discussion

3.1. Microwave spark ignition assisted graphene synthesis and characterization

Microwave irradiation is a powerful tool for heating. Graphite displays strong microwave absorption because of its low resistance, with a dramatic temperature increase accompanied by luminous sparks [14]. Earlier report reveals that the microwave spark ignition of graphite results in the formation of graphene [27]. In this work, new and simple strategy is explored to synthesize graphene-silver nanoparticle hybrid using the natural graphite and silver precursors with the assistance of microwave spark ignition. In a typical experiment, natural graphite flakes are mixed with hydrogen peroxide solution and ammonium peroxidisulfate in the ratio of 1:2:0.1 (w/w) followed by the addition of silver nitrate solution and poly (ethylene glycol) solution. The resultant mixture is subjected to irradiation for 60 s, resulting in bright sparks with the generation of water vapors and intense heat release. The above synthesis process is environmental friendly as microwave radiation is a green energy source and the chemicals used in the process are eco-friendly, which could be removed by repeated washing with water. When graphite and silver precursors are subjected to microwave spark ignition in the presence of ammonium peroxidisulfate and hydrogen peroxide, it is expected that the reaction takes place in three major steps though the satisfactory explanation is elusive at this moment. A possible sequence of steps resulting in the formation of graphene-silver nanoparticle hybrid is shown in Fig. 1. In the first step, under the microwave radiation, ammonium peroxidisulfate decomposes releasing oxide radicals, which initiates the radical induced cutting along the edges and surface defects of the graphite sheets. Earlier report reveals that silver ion catalyzes the decomposition reaction of ammonium peroxidisulfate during which the existing silver ion state is converted from Ag^+ to Ag^{3+}

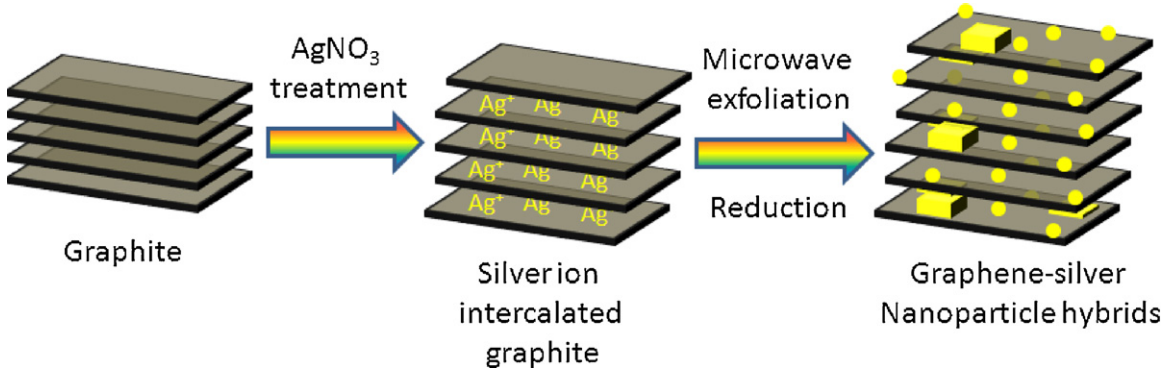

Fig. 1. Schematic representation showing the synthesis process of graphene-silver nanoparticle hybrids.

state with the regeneration of Ag^+ state on completion of reaction [28]. Since the silver ion catalyzes the ammonium peroxidisulfate decomposition, in the present study, it is expected that addition of silver ion accelerates the radical induced cutting of graphite edges in the first step. In the second step, the regenerated silver ions get intercalated between the graphene platelets as well as adsorbed onto the functional groups (—COOH) generated on the edges. It is also expectable that part of the silver ions intercalated between the graphene sheets undergo reduction reaction leading to the formation of silver nanostructures due to the presence of polyethylene glycol in the reaction mixture [29]. In the last step, the violent release of heat by the graphite flakes resulted in the rapid boiling of the hydrogen peroxide solution and water resulting in the expansion of graphite sheets to graphene layers. Though the exact mechanism by which silver nanoparticles generated at this stage is unknown, it is expected that initially formed silver nanostructures acts as the catalyst for H_2O_2 decomposition leading to the formation of superoxide's, which in turn reduces the residual silver ions (Ag^+) to silver nanoparticles [30,31].

The successful formation of the silver nanoparticles between the graphene layers are corroborated using X-ray photoelectron spectroscopy (XPS) and Fourier Transform Infrared Spectroscopy (FT-IR) characterization. Fig. 2a shows the X-ray photoelectron spectroscopic (XPS) results of graphene-silver nanoparticle hybrids. The survey scan results of the synthesized material shows a strong peak at 285 eV along with small peaks at 370 eV and 530 eV that are correspond to the C1s, Ag3d and O1s spectra of graphene-silver nanoparticle hybrid. High resolution of spectra of C1s spectra shows three peaks that can be corroborated to C—C, C—H (284.5 eV), —C—O (286 eV) and —COO (288 eV) present on the graphene surface (Fig. 2b). High resolution Ag3d spectra show two distinct peaks at 367.5 and 373.5 eV that are correlated to $Ag3d_{5/2}$ and $Ag3d_{3/2}$ (Fig. 2c). These peak values are typical values of Ag0, confirming the formation of silver nanoparticles on the graphene surface.

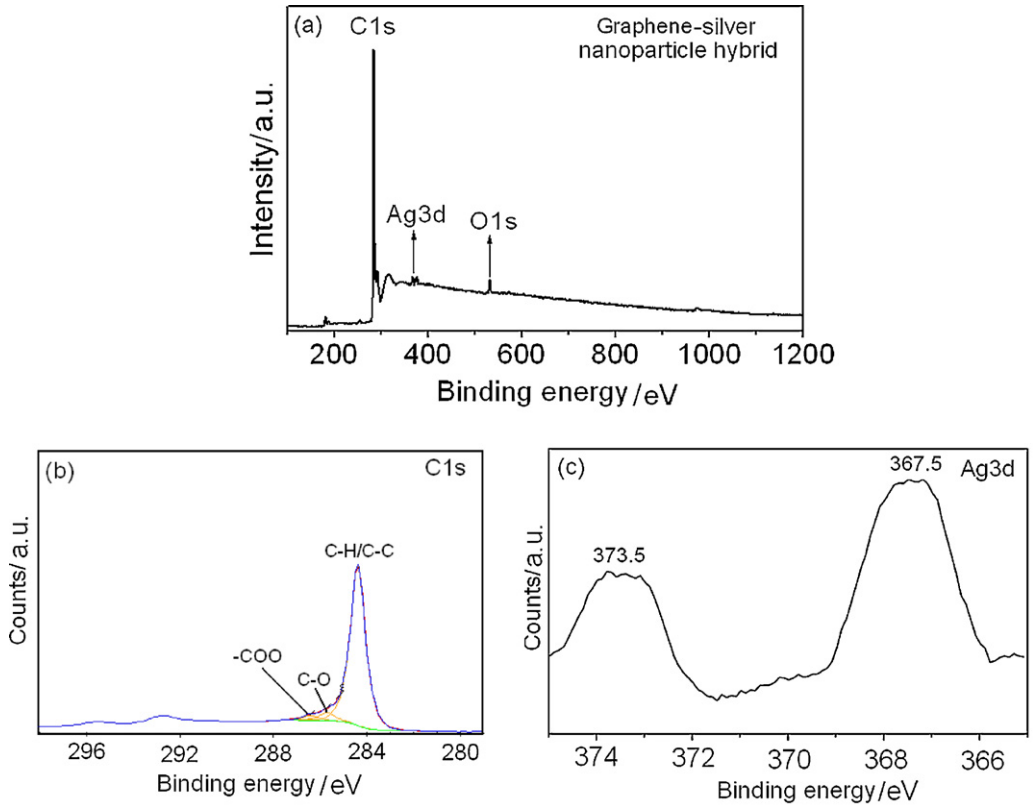

Fig. 2. XPS survey scan (a) and high resolution spectra of C1s (b) and Ag3d (c).

Table 1
Average d-spacing, lattice parameters and crystallite sizes of various facets of silver nanoparticles anchored on graphene nanosheets.

Nanoparticles	2θ of the intense peak (°)	Facets	d-Spacing (nm)	Lattice parameter (a) (nm)
Ag	38.2	(1 1 1)	0.235	0.407
	44.4	(2 0 0)	0.204	0.407
	64.6	(2 2 0)	0.144	0.407
	77.6	(3 1 1)	0.123	0.408
Ag_2O	54.8	(2 2 0)	0.165	0.470

Taking into account the relevant sensitivity factors, semiquantitative analysis of high resolution data gave a composition of 92.8% C, 6.3% O and 0.9% Ag in the graphene-silver nanoparticle hybrid. Relatively higher amount of oxygen content in the graphene-silver nanoparticle hybrid corroborates the formation of oxygen functionalities (—C═O) generated during the hydrogen peroxide decomposition reactions as proposed earlier. These observations are further supported by FT-IR results that show a sharp transmittance peak at 1710, 1365 and 1221 cm^{-1}, which are corroborated to —COO, C—O—C and C—OH groups present in the nanoparticle hybrids (Fig. 3). The relative amount of silver nanoparticles present in the graphene-silver nanoparticle hybrid is determined using TGA, by carrying out the thermal degradation in air environment (Fig. not shown). Significant weight loss occurs due to the degradation of graphene sheets on exposure to air at high temperature resulting in a residual weight of 23%, which can be corroborated to the relative concentration of silver in graphene-silver nanoparticle hybrids.

X-ray diffraction (XRD) pattern of graphene-silver nanoparticle hybrid is presented in Fig. 4. It shows four major diffraction peaks at 2θ = 38.9°, 44.4°, 65° and 78° along with the broad and diffused diffraction peak at 2θ = 24.0° (Fig. 5 (inset) and at 2θ = 54.8°).

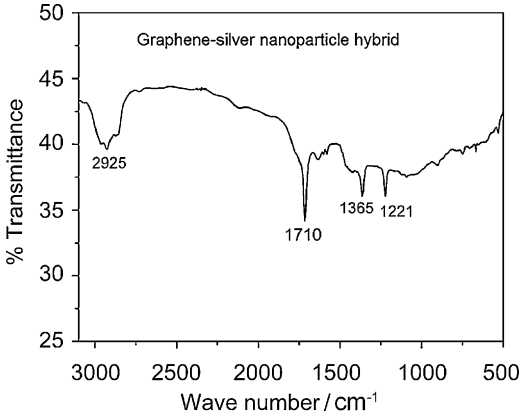

Fig. 3. FT-IR result of graphene-silver nanoparticle hybrid.

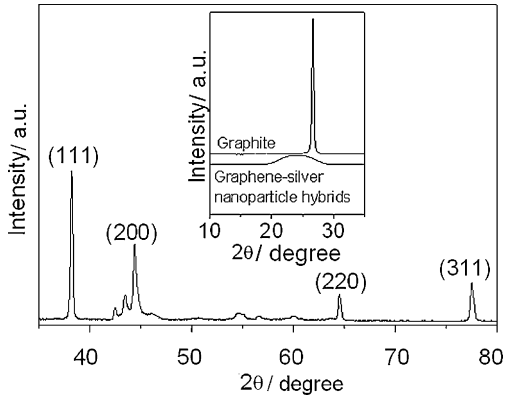

Fig. 4. XRD result of graphene-silver nanoparticle hybrid.

According to JCPS cards No. 04-0783, these peaks are indexed to (1 1 1), (2 0 0), (2 2 0) and (3 1 1) reflections of silver nanocrystals with face centered cubic symmetry, whereas the diffused diffraction peaks at 2θ = 24° and 54.8° are attributed to the (0 0 2) reflections of graphene nanosheets and (2 2 0) cubic planes of silver oxide (Ag_2O) nanostructures (JCPDS Card No. 12-0793). It is interesting to note certain new peaks at 2θ values of 42.6° and 43.5° along with the (2 0 0) reflection (2θ = 44.4) of FCC silver nanocrystals. Though the *hkl* reflections of these diffraction peaks are still unknown, a recent report revealed that these peaks may be attributed to Ag_xO nanoparticles with defective cubic Ag_2O structure with smaller d-spacing values [32]. The ratio of diffraction peaks of silver nanocrystals corresponding to (2 0 0)/(1 1 1) lattices and (2 2 0/(1 1 1) are calculated and it is observed to be 0.51 and 0.27, which are relatively higher compared to the conventional values ((2 0 0)/(1 1 1) = 0.40; (2 2 0)/(1 1 1) = 0.25) reported in JCPDS file No. 04-0783. The slightly higher value is attributed to the formation of silver nanocubic structures along with the formation of spherical nanoparticles. The average d-spacing and crystallite sizes of various facets are calculated using Bragg's and Debye–Scherrer equation [33] and the results are tabulated in Table 1. The calculated lattice cell parameters are 4.07 Å and 4.7 Å for Ag and Ag_2O nanoparticles and these values are quite consistent with the reported data (JCPDS file No. 04-0783 & JCPDS Card No. 12-0793). The diffraction peak intensity corresponding to (0 0 2) reflections drastically reduced and shifted to lower angle for microwave synthesized graphene-silver nanoparticle hybrids compared to graphite corroborating the decrease in thickness (L_c) of graphite crystallites (Fig. 5 (inset)). The average d-spacing of the graphene-silver nanoparticle hybrid calculated using the Bragg's law is approximately 0.370 nm, while for natural graphite it is 0.335 nm. The calculation of the number of graphene layers by fitting the (0 0 2) reflection is quite unreliable in the present case as the (0 0 2) diffraction peak is relatively broad revealing the presence of graphene nanosheets with varying d-spacing values. Fig. 5a and b shows the typical scanning electron microscopic (SEM) results of graphene-silver nanoparticle hybrids at two different magnifications. SEM images reveal a crumbled and scrolled morphology of graphene sheets (Fig. 5a) with distributed silver nanoparticles embedded within the graphene sheets (Fig. 5b). Fig. 5c–f shows the typical low and high magnification transmission electron microscopy (TEM) results of graphene-silver nanoparticle hybrids. The multilayer stacking arrangement of graphene structures consisting of uniformly distributed silver nanoparticles with approximately ~10 nm size along with few nanoparticles with larger particle sizes (~40 nm) embedded both at the edges as well as between the graphene layers (Fig. 5c). Histogram results corroborated that the particle size distribution is relatively broad with maximum distribution approximately at 10 nm (Fig. 5c (inset)). This fact is further confirmed from the high resolution TEM images (HR-TEM) of silver nanoparticles embedded within the curly and corrugated graphene nanosheets (Fig. 5d). The corrugated morphology clearly depicts the existence of the nano-voids in the graphene nanosheets (Fig. 5d (inset)). Fine distribution of silver nanoparticles within few graphene layers as well as its presence at the edges can be clearly visualized using TEM images (Fig. 5e and e (inset)). Radical induced cutting of graphite resulted in the formation of carboxylic groups, which acts as functional active

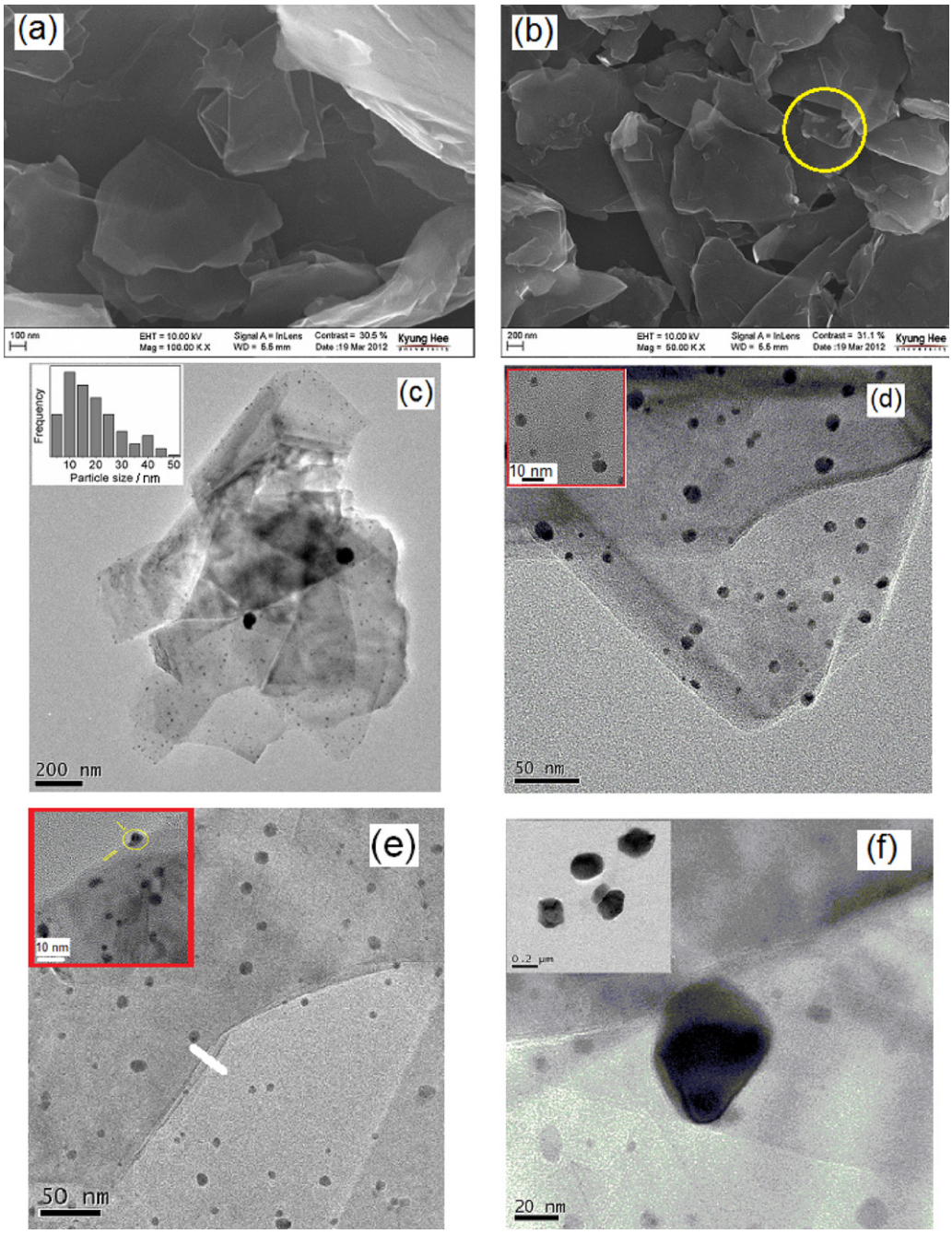

Fig. 5. SEM (a and b) and TEM (c–f) images of graphene-silver nanoparticle hybrids.

sites for silver ion adsorption and subsequent formation of silver nanoparticles as proposed earlier. Fig. 5f shows the HR-TEM image of silver nanocubic structure (~40 nm) embedded between the multilayered graphene nanosheets. To understand the formation mechanism of graphene-silver nanoparticle hybrids, an attempt has been made to synthesize silver nanoparticles using the silver precursors in the absence of graphite using microwave irradiation. The average particle sizes of the synthesized silver nanoparticles are observed to be 100–200 nm, which are significantly higher compared to the average particle size of silver nanoparticles, formed in the graphene-silver nanoparticle hybrids. From these results, it is quite evident that the microwave radiation of silver precursors in the presence of graphite not only resulted in the formation of graphene but also resulted in the significant reduction of the particle sizes of nanoparticles formed during the process. As visualized from TEM images, since few silver nanoparticles with the average particle size of ~40 nm are also embedded between the graphene sheets, it is quite expectable that certain degree of graphite is exfoliated with interlayer spacing greater than 40 nm during microwave spark ignition process.

Raman spectroscopy is a powerful tool for characterizing graphene derived materials. Micro-Raman spectra of dried dispersion of graphene and graphene-silver nanoparticle hybrids are shown in Fig. 6. The characteristic D and G bands appear at around 1320 and 1579 cm^{-1}, respectively. The former relates to the breathing mode of k-point photons of A_{1g} and the latter concerns the tangential stretching mode of E_{2g} phonon of sp^2 carbon atoms [34]. The G band position of the microwave synthesized graphene shifted to 1579 cm^{-1} with significant peak broadening, when compared to the pristine graphite (1575 cm^{-1}) due to

Table 2
Raman spectroscopy data and calculation of crystallite sizes of microwave synthesized graphene and graphene-silver nanoparticle hybrids.

Sample	Band position (cm^{-1})			I_D/I_G	I_{2D}/I_G	L_a (nm)
	D	*G*	2*D* (*G*′)			
Graphene	1320	1579	2638	0.93	0.67	18
Graphene-silver nanoparticle hybrids	1321	1578	2642	0.71	0.29	24

the decrease in the number of graphene layers [27,35]. In addition, the D band at 1320 cm^{-1} becomes prominent in microwave synthesized graphene, indicating the reduction in size of the in-plane sp^2 domains, possibly to the increase in surface defects due to the microwave induced oxidation. In case of graphene-silver nanoparticle hybrid, though there is no significant variation in the G band position (~1578 cm^{-1}), the band intensity increases significantly with the formation of small hump at 1610 cm^{-1}, when compared to microwave synthesized graphene. Appearance of this small hump may be attributed to the presence of trace amount of monolayer graphene in these hybrid materials [36]. The rise in band intensity is corroborated to the fine distribution of silver nanoparticles in the graphene matrix that induces surface enhanced Raman scattering (SERS) activity. The possible mechanisms that contribute to these surface enhancement in such systems are electromagnetic and charge-transfer mechanisms that exists between graphene and silver nanoparticles [37]. The intensity of D band also increases slightly for graphene-silver nanoparticle hybrids with blue shift to higher wavenumber (1322 cm^{-1}), when compared to the microwave synthesized graphene (Table 2). Interestingly, the intensity ratio (I_D/I_G) ratio, which is the measure of surface defects decreases from 0.93 (graphene) to 0.71 (graphene-Ag nanoparticle hybrids) corroborating the minimal effect of the silver nanoparticle growth on the graphene etching [36]. Appearance of broad 2D band (~2640 cm^{-1}) for both microwave synthesized graphene and graphene-silver nanoparticle hybrids confirm the existence of multilayered graphene nanostructures (Fig. 6 (inset)). The intensity of the peak corresponding to 2D band decreases for graphene-silver nanoparticle hybrids compared to graphenes ($I_{2D/G}$ for graphene is 0.67 and for graphene-silver is 0.29), which can be possibly related to the decrease in surface defects due to the doping of silver nanoparticles between the graphene platelets [38,39]. The crystalline domain sizes of the microwave synthesized graphene and graphene-silver nanoparticle hybrids are calculated by employing the following equation [40]

$$L_a = (2.4 \times 10^{-10})\lambda_{laser}^4 \left(\frac{I_D}{I_G}\right)^{-1}$$

The in-plane crystallite sizes (L_a) decreases from 114 nm (graphite) to 18 nm (graphene), when graphite is exfoliated using microwave radiation. However, in-plane crystallite size slightly increases to 24 nm (graphene-silver nanoparticle hybrids) confirming the decrease in surface defects due to silver nanoparticles between the graphene platelets [40].

3.2. Electrochemical characterization

The electrochemical properties of the graphene-silver nanoparticle hybrids as anodes in lithium-ion cells are evaluated via constant current charge/discharge cycling in the potential range of 0.01–3.0 V at 0.1 C rate. The cycleability of the graphene electrodes is examined under long-term cycling over 50 cycles, which demonstrated a good cyclic performance and reversibility (Fig. 7). Graphene-silver nanoparticle hybrid based anode materials delivered a specific capacity of 827 mAh g^{-1} in the initial discharge process and a reversible capacity of 780 mAh g^{-1} in the first charging process. This value is significantly higher compared to graphene anodes prepared through microwave spark ignition (discharge capacity, 580 mAh g^{-1} and reversible capacity is 498 mAh g^{-1}) [27]. The higher Li storage capacity for the graphene-silver nanoparticle hybrid is attributed to the synergetic contribution of graphene and silver in the lithium storage process. As indicated by the theoretical study, if all graphene nanosheets are strictly monolayer, the maximum lithium storage capacity of graphene is 744 mAh g^{-1}, corresponding to the formation of the Li_XC. Graphene-silver nanoparticle hybrids prepared via microwave process contains 23 wt% silver and therefore the theoretical capacity of graphene-silver nanoparticle hybrids can be calculated as

$$\text{Total capacity} = C_{graphene} \times 77\% + C_{silver} \times 23\%$$

where $C_{graphene}$ is the storage capacity of graphene and C_{silver} is the storage capacity of silver nanoparticles (820 mAh g^{-1}) [41]

$$\text{Total capacity} = 744 \times 0.77 + 820 \times 0.23 = 761.5 \text{ mAh g}^{-1}$$

Slightly higher value of initial storage capacity for graphene-silver nanoparticle hybrid is attributed to the additional storage of Li-ion in the nano-voids present in the graphene surface or micrpores generated in the graphene surface during the oxidation-reduction process or nano-cavities generated due to the partial insertion of silver in the graphene surface. Although, graphene

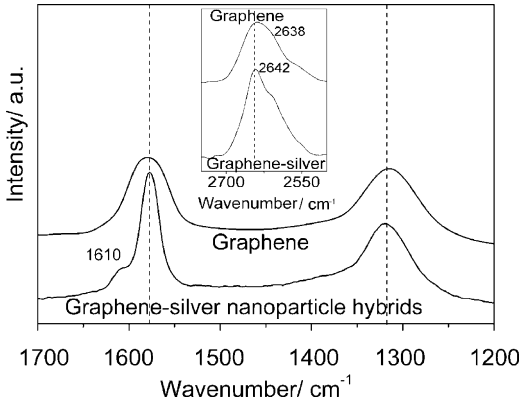

Fig. 6. Raman spectroscopic results of graphene and graphene-silver nanoparticle hybrids.

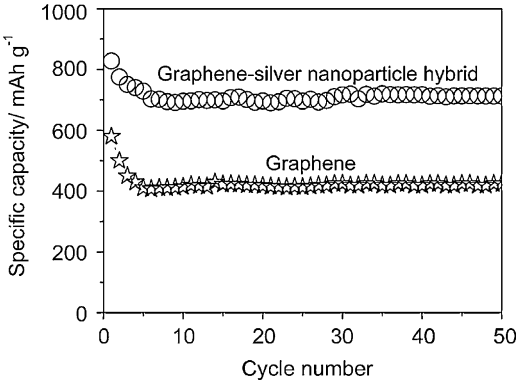

Fig. 7. Cyclic performance of graphene and graphene-silver nanoparticle hybrid at 0.1 C rate.

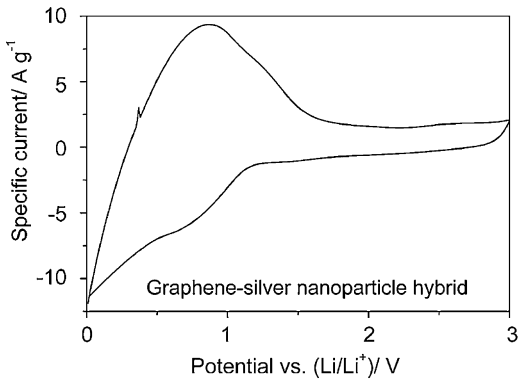

Fig. 8. Cyclic voltammogram of graphene-silver nanoparticle hybrid.

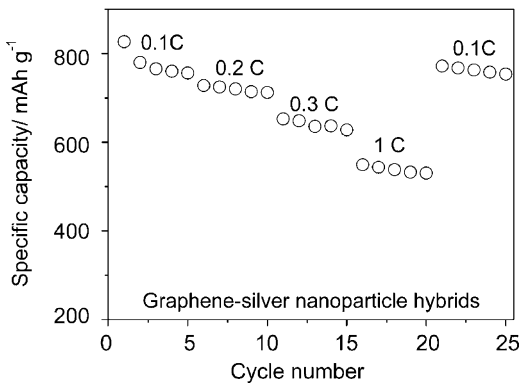

Fig. 9. Cyclic performance of graphene and graphene-silver nanoparticle hybrid at various C rates.

nanosheets in the nanoparticle hybrids are not entirely monolayer, we have achieved a reversible lithium storage capacity of 780 mAh g^{-1} in the second cycle, which is comparable to the theoretical capacity. The electrochemical behavior of silver with lithium have been studied extensively by Park et al. [42] and they showed that the silver nanoparticles exhibit excellent electrochemical reversible reaction with first discharge and charge capacities of 1158 and 727 mAh g^{-1}, which is quite comparable with the present results. After 50 cycles, the graphene-silver nanoparticle hybrid electrodes still maintained a specific capacity of 714 mAh g^{-1}, which represents a much enhanced performance than that of graphene (specific capacity, 420 mAh g^{-1}) or graphite electrodes (specific capacity, 372 mAh g^{-1}). The higher reversible capacity of graphene-silver nanoparticle hybrid compared to graphene or silver (reversible capacity, 315 mAh g^{-1}) [16] is ascribed to the confinement of silver nanoparticles at the graphene edges and between the graphene layers. Confinement of nanoparticles prevents the nanoparticle aggregation during charge/discharge cycles and thereby maintains the constant charge/discharge profiles [41], whereas the presence of silver nanoparticles between the graphene layers prevents the aggregation of graphene layers leading to the enhanced lithium storage performance. In addition, the voids existing in graphene nanosheets can effectively buffer the volume expansion of silver, when reacting with lithium [43]. Consequently, cracking and pulverization of the electrode can be avoided, resulting in an enhanced cycling stability. Earlier report on graphite based electrodes reveal that the graphite retains about 81% (columbic efficiency) of its initial specific discharge capacity even after 50 cycles [44]. The discharge capacity of graphene anode materials prepared through microwave exfoliation decreased by 27.6% (columbic efficiency, 72.4%) in 50 cycles corroborating its irreversible nature relative to graphite electrodes. Layering of silver nanoparticles between the graphene platelets resulted in the improvement of columbic efficiency (86%) revealing the enhanced reversible capacity behavior of graphene-silver nanoparticle hybrids. The irreversible nature of graphene electrodes compared to graphite may be attributed to the presence of residual oxygen containing functional groups in the nanopores of the graphene electrode that chemically reacts with the lithium ion resulting in the appreciable voltage hysteresis during the charging process. However, residual oxygen content in graphene-silver nanoparticle hybrids are relatively lesser compared to graphene electrodes corroborating the reduction in the voltage hysteresis during the charging process and also the presence of silver nanoparticles that improves the electrochemical performances. Further improvements are expected by tuning the morphology of the silver nanoparticles between the graphene platelets and graphitic structure of the graphene sheets by adjusting the microwave processing parameters.

To identify all of the electrochemical reactions in graphene-silver nanoparticle hybrids, cyclic voltammetry (CV) is conducted on the cell with graphene-silver electrode at ambient temperature in the 0.0–3.0 V range and a scan rate of 0.1 mV s^{-1} (Fig. 8). In the first cycle, a peak observed at around 1.0 V can be attributed to the irreversible reaction with the electrolyte. Earlier reports reveal that silver forms alloy with lithium with the electrochemical reaction mechanism as depicted below [45,46].

It is well known that reduction curves in Fig. 8 represent the lithium intercalation, which can be represented as

$$3Li^{\oplus} + C + 3e^{-} \rightarrow Li_3C$$

In addition, alloy reaction proceeds on the surface of silver nanoparticle sites on graphene surface as

$$Ag + Li^{\oplus} + e^{-} \rightarrow Ag\text{–}Li$$

The oxidation curves in the CV represent the lithium de-intercalation and it can be expressed as reverse of reduction reaction as

$$Li_3C \rightarrow 3Li^{\oplus} + C + 3e^{-}$$

The oxidation reaction of Ag–Li alloy along occurred on the nanoparticle grafted graphene surface as

$$Ag\text{–}Li \rightarrow Ag + Li^{\oplus} + e^{-}$$

Apparently, the CV profile of graphene-silver nanoparticle hybrids looks quite similar to graphite based electrodes (Fig. 8). A small peak at around 0.37 V corroborates to the oxidation peak of Ag–Li alloy during Li-ion de-intercalation reaction.

The specific discharge capacities of graphene-silver nanoparticle hybrid based anode materials at various C-rates are shown in Fig. 9. As expected the discharge capacity decreases with increasing C-rates. For instance, the first specific discharge capacity of graphene-silver nanoparticle hybrid electrodes decreases to 728 mAh g^{-1} (0.2 C rate), 652 mAh g^{-1} (0.3 C rate) and 549 mAh g^{-1} (1 C rate) from 827 mAh g^{-1} (0.1 C rate). These values are relatively higher compared to graphite electrodes revealing its enhanced electrochemical performances.

4. Conclusions

In conclusion, we have demonstrated one pot synthesis route to produce graphene-silver nanoparticle hybrid based materials with the assistance of microwave spark ignition process. TEM observation revealed the successful formation of graphene-silver nanoparticle hybrid materials with nanoparticles of varying structures. XPS and Raman spectroscopic studies corroborated the existence of few surface defects on the synthesized nanoparticle

hybrids. Electrochemical measurements revealed that the anode materials synthesized through microwave spark ignition shows relatively good cyclic performances with higher reversible capacity ($714\,mAh\,g^{-1}$) relative to graphene or graphite based anode materials.

Acknowledgement

This work was supported by Kyung Hee University grant (KHU-20110248).

References

[1] A.S. Bernard, I.K. Shook, Journal of Chemical Physics 128 (2008) 094707.
[2] Y. Zhang, Y.W. Tan, H.L. Stormer, P. Kim, Nature 438 (2005) 201.
[3] N. Tombros, C. Jozsa, M. Popinciuc, H.T. Jonkman, B.J. van Wees, Nature 448 (2007) 571.
[4] K.S. Kim, Y. Zhao, H. Jang, S.Y. Lee, J.M. Kim, K.S. Kim, J.H. Ahn, P. Kim, J.Y. Choi, B.H. Hong, Nature 457 (2009) 706.
[5] Y. Wang, Y. Huang, Y. Song, X.Y. Zhang, Y.F. Ma, J.J. Liang, Y. Chen, Nano Letters 9 (2009) 220.
[6] Y.M. Lin, C. Dimitrakopoulos, K.A. Jenkins, D.B. Farmer, H.Y. Chiu, A. Grill, Ph. Avouris, Science 327 (2010) 662.
[7] Y. Zheng, G.X. Ni, C.T. Toh, M.G. Zeng, S.T. Chen, K.B. Yao, B. Özyilmaz, Applied Physics Letters 94 (2009) 163505.
[8] X.S. Li, Y.W. Zhu, W.W. Cai, M. Borysiak, B.Y. Han, D. Chen, R.D. Piner, L. Colombo, R.S. Ruoff, Nano Letters 9 (2009) 4359.
[9] F. Schedin, A.K. Geim, S.V. Morozov, E.W. Hill, P. Blake, M.I. Katsnelson, K.S. Novoselov, Nature Materials 6 (2007) 652.
[10] Y. Wang, Z. Shi, Y. Huang, Y. Ma, C. Wang, M. Chen, Y. Chen, Journal of Physical Chemistry C 113 (2009) 13103.
[11] P. Guo, H. Song, X. Chen, Electrochemistry Communications 11 (2009) 1320.
[12] Y. Liu, J.S. Xue, T. Zheng, J.R. Dahn, Carbon 34 (1996) 193.
[13] P. Poizot, S. Laruelle, S. Grugeon, L. Dupont, J.M. Tarason, Journal of Power Sources 97–98 (2001) 235.
[14] C.K. Chan, H. Peng, G. Liu, K. McIlwrath, X.F. Zhang, R.A. Huggins, Y. Cui, Nature Nanotechnology 3 (2008) 31.
[15] P. Poizot, S. Laruelle, S. Grugeon, L. Dupont, J.M. Tarason, Nature 407 (2000) 496.
[16] J.H. Ahn, Y.J. Kim, G.X. Wang, H.K. Liu, J. Metastab, Journal of Metastable and Nanocrystalline Materials 26 (26) (2005) 1.
[17] C.K. Chan, X.F. Zhang, Y. Cui, Nano Letters 8 (2008) 307.
[18] Y. Zou, Y. Wang, Nanoscale 3 (2011) 2615.
[19] G.X. Wang, Y. Chen, K. Konstantinov, M. Lindsay, H.K. Liu, S.K. Dou, Journal of Power Sources 109 (2002) 142.
[20] J.P. Maranchi, A.F. Hepp, A.G. Evans, N.T. Nuhfer, P.N. Kumta, Journal of the Electrochemical Society 153 (2006) A1246.
[21] J.K. Lee, K.B. Simth, C.M. Harner, H.H. Kung, Chemical Communications 46 (2010) 2025.
[22] G. Wang, B. Wang, X. Wang, J. Park, S. Dou, H. Ahn, K. Kim, Journal of Materials Chemistry 19 (2009) 8378.
[23] S. Yang, X. Feng, S. Ivanovici, K. Müllen, Angewandte Chemie International Edition 49 (2010) 8408.
[24] S.J. Park, R.S. Ruoff, Nature Nanotechnology 4 (2009) 217.
[25] S. Vadukumpully, J. Paul, S. Valiyaveettil, Carbon 47 (2009) 3288.
[26] V. Sridhar, J.H. Jeon, I.K. Oh, Carbon 48 (2010) 2953.
[27] A.M. Shanmugharaj, W.S. Choi, C.W. Lee, S.H. Ryu, Journal of Power Sources 196 (2011) 10249.
[28] C.V. King, Journal of the American Chemical Society 50 (1928) 2080.
[29] K. Mallick, M. Witcomb, M. Scurrell, Materials Chemistry and Physics 97 (2006) 283.
[30] Y. Ono, T. Matsumura, N. Kitajima, S.I. Furukumi, Journal of Physical Chemistry 81 (1977) 1307.
[31] A.M. Jones, S. Garg, D. He, N. Pham, T. David Waite, Environmental Science and Technology 45 (2011) 1428.
[32] W. Wei, X. Mao, L.A. Ortiz, D.R. Sadoway, Journal of Materials Chemistry 21 (2011) 432.
[33] B. Saner, F. Okyay, Y. Yurum, Fuel 89 (2010) 1903.
[34] F. Schedin, E. Lidorikis, A. Lombardo, V.G. Kravets, A.K. Geim, A.N. Grigorenko, K.S. Novoselov, A.C. Ferrari, ACS Nano 4 (2010) 5617.
[35] F. Tuinstra, J.L. Koenig, Journal of Chemical Physics 53 (1970) 1126.
[36] Z. Xu, H. Gao, H. Guoxin, Carbon 49 (2011) 4731.
[37] X.Q. Fu, F.L. Bei, X. Wang, S. O' Brien, J.R. Lombardi, Nanoscale 2 (2010) 1461.
[38] B.S. Kalanoor, P.B. Bisht, S. Akbar Ali, T.T. Baby, S. Ramaprabhu, Journal of the Optical Society of America B 29 (2012) 669.
[39] A. Das, S. Pisana, B. Chakraborty, S. Piscanec, S.K. Saha, U.V. Waghmare, K.S. Novoselov, H.R. Krishnamurthy, A.K. Geim, A.C. Ferrari, A.K. Sood, Nature Nanotechnology 3 (2008) 210.
[40] M.A. Pimenta, G. Dresselhaus, M.S. Dresselhaus, L.G. Cancado, A. Jorio, R. Saito, Physical Chemistry Chemical Physics 9 (2007) 1276.
[41] G.X. Wang, Y. Chen, L. Yang, J. Yao, S. Needham, H.K. Liu, J.H. Ahn, Journal of Power Sources 146 (2005) 487.
[42] C.-M. Park, H. Jung, H.-J. Sohn, Electrochemical and Solid-State Letters 12 (2009) A171.
[43] C. Wang, D. Li, C.O. Too, G.C. Wallace, Chemistry of Materials 21 (2009) 2604.
[44] G.F. Ortiz, R. Alcántara, P. Lavera, J.L. Tirado, Journal of the Electrochemical Society 152 (2005) A1797.
[45] W.C. Choi, D. Byun, J.K. Lee, B.W. Cho, Electrochimica Acta 50 (2004) 523.
[46] C.M. Park, J.-H. Kim, H. Kim, H.J. Sohn, Chemical Society Reviews 39 (2010) 3115.